

EXPERIMENTAL INVESTIGATION ON EFFICIENT HEAT COLLECTION OF ABOVEGROUND PIPES

by

Kaipeng WANG^a, Qimin LI^{a*}, Ke CHENG^a, and Jian WANG^{b,c}

^a School of Water Resources and Environment,
China University of Geosciences, Beijing, China

^b School of Civil Engineering, Southwest Jiaotong University, Chengdu, China

^c MOE Key Laboratory of High-Speed Railway Engineering,
Southwest Jiaotong University, Chengdu, China

Original scientific paper

<https://doi.org/10.2298/TSC190727423W>

Prospects for low-cost utilization and storage of solar energy are promising. In this study, the change of shallow geo-temperature was monitored, and the influence of solar radiation on shallow geo-temperature was discussed. Three series of field experiments on heat transfer of aboveground pipes were designed, and the variations of water temperature in the aboveground pipes were also monitored. According to the experimental data, the relevant factors affecting the water temperature inside the pipe (such as solar radiant intensity, pipe's material, pipe's spatial location, heat-accumulating wall and so on) were analyzed. Based on the field test, a 3-D model of aboveground pipe heat transfer was established to verify and temperature prediction was carried out. The results show that the water temperature in the pipe is most significantly affected by solar radiation, and is also related to the color of the pipe and its spatial position. The water temperature of galvanized steel pipe wrapped with black plastic film is the highest under solar radiation, and the optimum distance between the pipe and the heat-accumulating wall and the Earth's surface is, respectively, 0.90~1.25 times of the outer diameter of the pipe. The way the pipe is covered has a great influence on the water temperature inside the pipe. When the black and polyethylene pipe covered with the white plastic film is in the best spatial position, the highest heat of the three series of tests is obtained, and the difference between the water temperature inside the pipe and the atmospheric temperature reaches 36.3 °C.

Key words: solar thermal utilization, geo-temperature monitoring,
pipe heat collection experiment, numerical simulation,
temperature prediction

Introduction

Solar energy, as an eco-friendly, eternal [1] and environmentally friendly renewable energy, is favored by all countries in the world, as fossil energy is gradually consumed.

In China, Solar collectors are available in both evacuated tubular type and flat plate type, which of the former accounts for more than 95% of the domestic market [2]. Evacuated-tube solar hot water collector mainly relies on evacuated collector tube to convert solar energy into heat energy. In order to improve the performance of solar water heaters, different authors have conducted a lot of investigation by means of experiments. In the past few decades,

* Corresponding author, e-mail: qiminli@163.com; qiminli@cugb.edu.cn

the performance and structure of solar collectors were widely investigated and modified by many researchers [3-8], obtaining the best method to improve the thermal efficiency. Yakup and Malik [9] investigated the optimum tilt angle and orientation (surface azimuth angle) for the solar collector in Brunei Darussalam by establishing mathematical models to estimate the total solar radiation on a tilted surface. Zhao *et al.* [10] investigated that it is most reasonable to install collectors with seasonal tilt-angle in Lanzhou, China, changing the tilt-angle twice a year. Despotovic *et al.* [11] investigated the optimum tilt angle by searching for the values for which the solar radiation on the collector surface is maximum for a particular day or a specific period, determining the biannual, seasonal, monthly, fortnightly, and daily optimum tilt angles. In recent years, phase change materials (PCM), have been well developed and because of their superior heat storage capacity, so their integration with solar collectors produced better results [12]. Lin *et al.* [13] conducted an outdoor experimental investigation of integrated PCM-flat plate solar collector at various inclination angles (10°, 20°, and 30°). They found that 0.5 kg per minute water flow rate and 10° to 20° inclination angles with PCM can provide promising 38 °C hot water temperature for daytime demand with 52 ± 2.2 % efficiency. Abuska *et al.* [14] investigated the effect of using aluminum honeycomb core on the solar air collector thermal performance regarding heat storage with PCM under natural-convection conditions. They found that the production of useful energy in the novel solar air collector lasted 469 minute and 539 minute longer than collector with a flat absorber plate, respectively.

There are also some authors who have done a lot of research by means of numerical simulation [15-17]. Alfaro-Ayala *et al.* [18] considered the buoyancy effects in the numerical simulation of the water-in-glass evacuated tube solar collector. The simulated results show that the outlet temperature and thermal efficiency of the solar collector using the model of Boussinesq approximation is closer to the experimental data than those obtained using the model of variation of the properties with temperature. Morrison *et al.* [19] discussed the factors influencing the operation of water-in-glass collector tubes, and presented a numerical study of water circulation through long single-ended thermosyphon tubes. Preliminary numerical simulations have shown the existence of inactive region near the sealed end of the tube which might influence the performance of the collector. Selmi *et al.* [20] simulated and analyzed the problem of flat plate solar energy collector with water flow, considering the radiative heat transfer between tube surface, glass cover, side walls, and insulating base of the collector as well as the mixed convective heat transfer in the circulating water inside the tube and conduction between the base and tube material. The simulated results show that the outlet temperature of water is compared with experimental results and there is a good agreement. Charvat *et al.* [21] investigated influence of latent heat thermal energy storage integrated with the solar absorber plate through lab experiments and computer simulations. The result indicates that solar absorber plate containing a paraffin-based PCM has the potential to reduce the outlet air temperature fluctuations when the solar radiation intensity quickly changes.

Even though the thermal efficiency has been improved, the use of solar collector tubes becomes economically infeasible with the increase of service time. Ayompe *et al.* [22] conducted a year-round monitoring of the performance of flat plate and heat pipe of evacuated tube solar collector. The results showed that the two systems were not economically feasible. Because the effective use of ground reflected light and ground heat flow is not considered, the cost of solar water heaters is high, and it is economically unfeasible when producing large quantities of hot water. Combining the advantages of solar energy and shallow geothermal energy, this paper designs and conducts heat transfer test of aboveground pipes in Haidian district of Beijing, analyses test data, establishes the heat transfer numerical model and temperature pre-

dictive model, and proposes a low-cost method to improve water temperature efficiently, which provides experimental support for large-scale utilization of solar energy.

Practical experiment and monitoring design

Introduction of Haidian district

Haidian district is located in the northwest of Beijing, the capital of the People's Republic of China, which of district borders is between 39°53'~40°09' N latitude and 116°03'~116°23' E longitude. The climate in Haidian district belongs to the warm temperate semi-humid semi-arid continental monsoonal climatic zone with an average annual temperature of 12.5 °C, an extreme minimum temperature of -21.7 °C, an average temperature of 25.8 °C in July, and a maximum temperature of 41.6 °C. The annual sunshine is 2662 hours and the frost-free period is 211 days. The annual average precipitation is 628.9 mm, concentrated in June-August in summer. The summer rainfall is 465.1 mm, accounting for 70% of the annual precipitation. The precipitation in December to February in winter is the least, accounting for only 1%. Therefore, the climatic characteristics of this area are more rain in summer, drought in spring and autumn, and cold and dry in winter.

Design of geo-temperature monitoring

In order to investigate the variation of stratigraphic temperature at different burial depths, the author selected a relatively flat and open space in Haidian District of Beijing, where is no shadows such as trees and buildings. The properties of the site soil are ordinary silty clay in Beijing area. Five holes were drilled into the soil at the surface, with a diameter of 40 mm and a drilling depth of 0.3 m, 0.6 m, 0.9 m, 1.2 m, and 1.5 m, respectively, and the spacing of each hole was 1.0 m. Then the temperature probes of the intelligent temperature recorder (HZ-TJ1) were embedded in the boreholes with depths of 0.01 m, 0.30 m, 0.60 m, 0.90 m, 1.20 m and 1.50 m, respectively, and the holes are sealed by compaction with the original soil. The data recording interval of the geothermal monitoring experiment was 15 minute, and the hourly temperature and humidity in Haidian District of Beijing were also recorded.

Design of heat transfer test for aboveground pipe

Experimental material

The main experimental instruments used in the test include: Multi-point soil temperature recorder HZ-TJ1, its temperature measuring range: -40~120 °C, accuracy: ± 0.2 °C; galvanized steel pipes; polyethylene (PE) plastic pipes; black and white plastic film and foam scaffolds. The specifications of pipes are shown in tab. 1.

Table 1. The specifications and parameters of pipes

Pipe type	Color	Length, L [mm]	Inner diameter, DN , [mm]	outer diameter, D [mm]	Wall thickness, δ [mm]
Galvanized steel pipes	White	750	25	33.4	4.2
PE plastic pipes	Black	750	26	32	3.0

Experimental site

In this series of experiments, the large sandpit in the university of the playground was used as test site, as shown in fig. 1. The particle size distribution test of sand in sandpit was car-

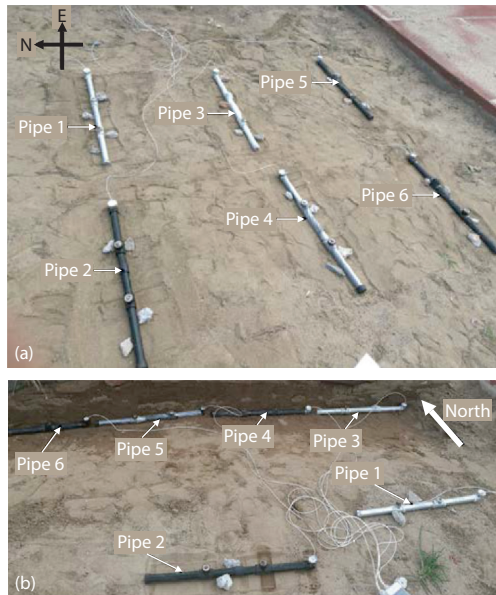


Figure 1. Test site

ing that the site sand is medium sand. According to the experiments, the distributed curve of sand size is drawn as fig. 2, and the calculative results show that the coefficient of uniformity $C_u = 9.67 > 5$, the coefficient of curvature $C_c = 2.94$, and $1 < C_c < 3$. The experiment proves that there are large and small particles in the sand, the particle size is relatively dispersed, the gradation and compactness are both good.

Treatment of experimental pipes

Two galvanized steel pipes and PE plastic pipes are, respectively, wrapped in black and white plastic films, and the remaining two are not treated. The number of experimental pipes are Pipe 1 is the galvanized steel; Pipe 2 is the PE plastic pipe; Pipe 3 is the galvanized steel pipe wrapped with white plastic film; Pipe 4 is the PE plastic pipe wrapped with white plastic film; Pipe 5 is the galvanized steel pipe wrapped with black plastic film; Pipe 6 is the PE plastic pipe wrapped in black plastic film; Pipe 7 is the galvanized steel pipe covered with white plastic film; Pipe 8 is the PE plastic pipe covered with white plastic film; Pipe 9 is the galvanized steel pipe covered with black plastic film; Pipe 10 is the PE plastic pipe covered with black plastic film.

Experimental method

On the basis of full consideration of the influencing factors, the following three-stages of experiments were carried out.

In the first stage, considering the overhead impact test: all the pipes are filled with water and placed on the sand ground with a horizontal spacing of 1.0 m. Six temperature probes of soil temperature recorder HZ-TJ1 are placed in the pipes to measure the change of water temperature. The measuring time is 12 hours, which is from 7:00 a. m. to 19:00 p. m. and the recording interval of is 15 minutes. Under the condition that the measuring time and horizontal spacing remain unchanged, the pipes' bottom of Pipe 3, Pipe 4, Pipe 5, and Pipe 6 are all overhead to the sand ground height of 20 mm on the second day. With the increase of test days, the

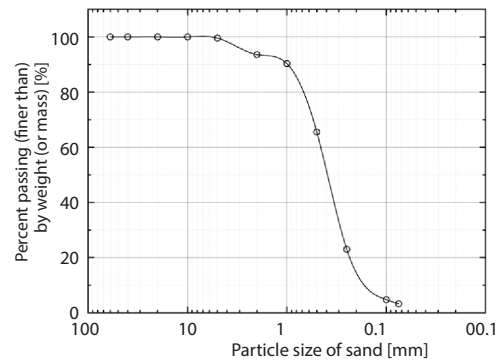


Figure 2. Curve of grain size distribution

ried out by sieve analysis method. The experimental results show that the mass of particles with particle size greater than 0.5 mm accounts for 34.48% and less than 50% of the total mass, while the mass of particles with particle size greater than 0.25 mm accounts for 76.98% and more than 50% of the total mass, indicat-

four pipes are all arranged at 30 mm, 40 mm, 50 mm, and 65 mm for measurement. Pipe 1 and Pipe 2 are always placed on the surface of sand ground for reference.

In the second stage, the influence test of the heat-accumulating wall is considered: the heat-accumulating wall is set on the ground of the sand ground, which of the size is 4 m long, 0.3 m wide, and 0.55 m high and the surface is treated with sand. The lengthwise direction of wall is arranged along the east-west direction. Pipe 1 and Pipe 2 are always placed on the sand ground as the control group after being filled with water, with a horizontal distance of 1 m, which of lengthwise direction are arranged along the east-west direction. The lengthwise directions of the Pipe 3, Pipe 4, Pipe 5, and Pipe 6 are consistent with the lengthwise directions of the wall. It is noted that the bottom of Pipe 3, Pipe 4, Pipe 5, and Pipe 6 is X mm from the sand ground and Y mm from the heat-accumulating wall. The four pipes are all arranged at (0, 0) and the measurement is started. The measuring time is 12 hours, that is, from 07:00 a. m. to 07:00 p. m. On the second day of the experiment, they are all arranged at (20, 20) for measurement. With the increase of test days, the four pipes are all arranged at (30, 30), (40, 40), (50, 50), and (65, 65) for measurement.

In the third stage, the test of coverage is considered: Pipe 1 and Pipe 2 are always placed on the sand ground after filling with water as control group. The experimental method of Pipe 7, Pipe 8, Pipe 9, and Pipe 10 is basically the same as that of the second stage, except that the spatial position of the pipe-line is different. The specific spatial locations are: (-35, 100), (-15, 100), (0, 100), (20, 100), (40, 100), (65, 100). The position of the pipe relative to the ground and wall is shown in fig. 3

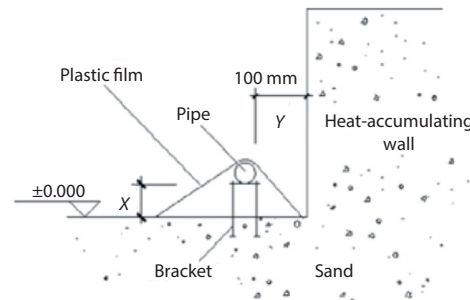


Figure 3. Cross-section of plastic film covering pipe experiment

Experimental principle and monitoring analysis

Experimental principle

According to the thermal balance of the boundary surface, the heat transfer on the surface of the pipe follows Fourier's law and Newton's cooling formula:

$$-\lambda \frac{\partial T}{\partial n} = H(T_w - T_f) + q_r \quad (1)$$

where λ [$\text{Wm}^{-1}\text{C}^{-1}$] is the thermal conductivity, n – the normal direction of the pipe's surface, H [$\text{Wm}^{-2}\text{C}^{-1}$] – the heat transfer coefficient, T [$^{\circ}\text{C}$] – the temperature, T_w [$^{\circ}\text{C}$] – the wall temperature of the pipe, T_f [$^{\circ}\text{C}$] – the fluid temperature, q_r [Wm^{-2}] – heat flux density, being related to the fourth power of temperature.

The radiant heat transfer on the surface of the pipe takes into account the long-wave radiation between pipe-line and atmosphere, the long-wave radiation between pipe-line and ground, and the radiative heat transfer between the pipe and the wall:

$$q_r = \varepsilon_f \sigma (T_w^4 - T_s^4) \varphi_{ws} + \varepsilon_f \sigma (T_w^4 - T_g^4) \varphi_{wg} + \varepsilon_f \sigma (T_w^4 - T_h^4) \varphi_{wh} - I_a \quad (2)$$

where σ [$\text{Wm}^{-2}\text{K}^{-4}$] is the Stefan-Boltzmann constant with a value of $5.67 \cdot 10^{-8}$, ε_f – the superficial emissivity of the pipe, T_s [K] – the effective temperature of the sky, φ_{ws} – the angular coefficient between the pipe's surface and the sky, T_g [K] – the ground temperature, φ_{wg} – the angular coefficient between the pipe's surface and the ground, T_h [K] – the temperature of heat-accumu-

lating wall, ϕ_{wh} is the angular coefficient between the pipe's surface and the heat-accumulating wall, and I_a [Wm^{-2}] – the solar radiant intensity absorbed by the pipe.

Monitoring and analysis of shallow geo-temperature

The monitoring experiment of shallow geo-temperature was conducted from 12:00 p. m. on September 5 to 12:00 p. m. on September 8. The time interval of data recording was 15 minutes. It can be observed from figs. 4 and 5 that the variational tendency of soil temperature near the ground (-0.01 m) is basically consistent with that of solar radiant intensity on the day. With the increase of depth, the solar irradiance decreases, and the shallow geo-temperature also decreases, becoming stable under the influence of solar irradiance.

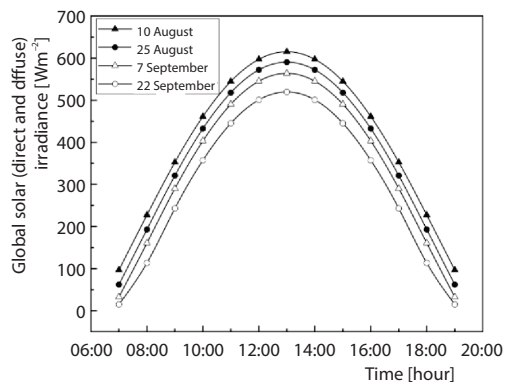


Figure 4. Curves of solar radiation intensity over time

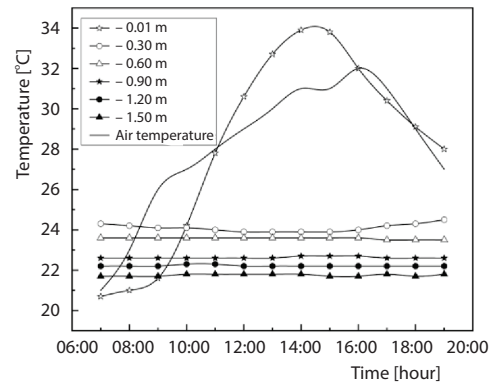


Figure 5. Curves of geo-temperature at different depths

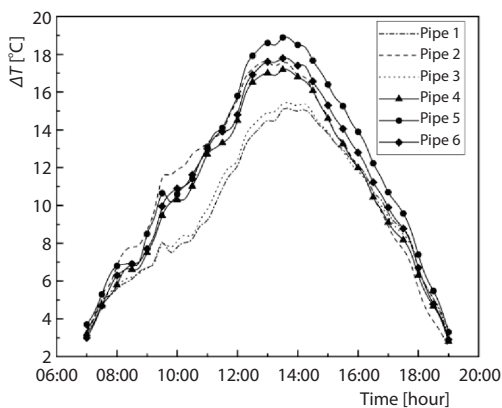


Figure 6. Curves of the difference between water temperature in pipes and air temperature on August 10

maximum temperature, and the temperature rises faster. The reason can be seen from the analysis: the surface of the black pipe can absorb as much visible energy in the solar energy as possible, which has a strong ability of heat absorption. The pipe can get more heat, so the water temperature is relatively high. While the white plastic film absorbs heat less than the black plastic film,

Heat transfer analysis of aboveground pipe

Pipes' color

The heat transfer test of aboveground pipe was carried out in the school playground from 7:00 on August 9 to 17:00 on September 23. A total of 1494 groups of experimental data were obtained. Figure 6 is the difference between the water temperature in the pipe and the real-time temperature on August 10, which shows that the water temperature of galvanized steel pipe wrapped with black plastic film (pipe 5) is generally higher than that of other pipes, followed by Pipe 6 and Pipe 2. Moreover, the maximum water temperature in the Pipe 5 is about 18.9 °C higher than the real-time maximum

so the thermal effect of the Pipe 3 and Pipe 4 is second. The heat gain of Pipe 1 is the least and the rise of water temperature is lower.

Spatial position of pipe

Because of the different weather conditions and the difference in atmospheric temperature, the water temperature in the pipe will also change. However, it can be observed from the experimental result that the spatial position of the pipe on the sand has a significant influence on the temperature of the water in the pipe. As shown in fig. 7, taking the Pipe 5 as an example, the influence of the spatial position of the pipe on the water temperature is analyzed by the difference between the measured temperature of the water in the pipe and the atmospheric temperature of the day. When the bottom of the pipe is 40 mm from the sand ground, the water in the pipe warms up faster, and the highest temperature difference can reach 20.9 °C. At the heights of 30 mm, 50 mm, and 60 mm from the sand ground, the water temperature changes similarly, while at 0 mm, the water temperature is relatively low.

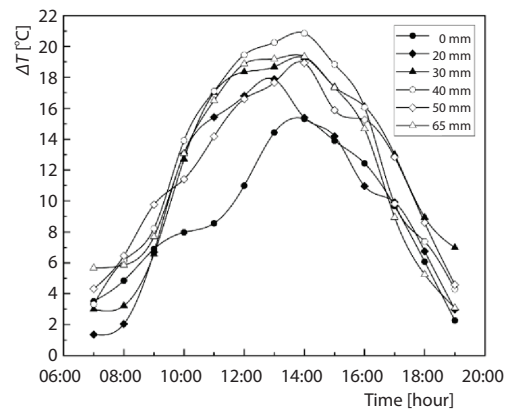


Figure 7. Curves of the difference between water temperature in pipes and air temperature at different heights from pipe bottom to ground

Heat-accumulating wall

Experiment has shown that heat-accumulating wall has a significant influence on the temperature of the water inside the pipes. In order to further explore the effect of heat-accumulating wall, the variation of the water temperature inside the pipes when the Pipe 5 is 40 mm from the wall space and the sand ground is compared with the experimental method which only places the pipe 5 at a height of 40 mm without the heat collecting wall. Figure 8 is obtained by making the difference between the measured water temperature and the real-time atmospheric temperature, which emerges that the role of the heat-accumulating wall is very obvious. After 13:00 p. m., at the same height, the temperature of water in the pipe with the heat-accumulating wall is about 5-10 °C higher than that without the heat-accumulating wall.

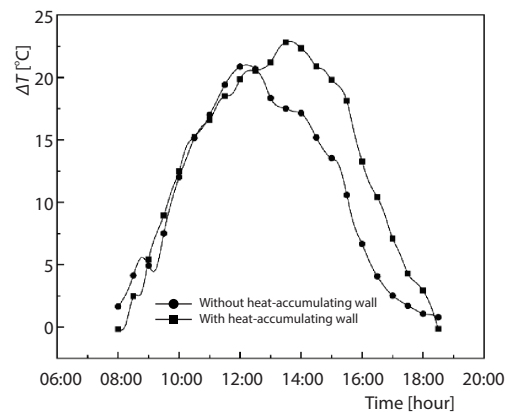


Figure 8. Contrast chart of water temperature in pipe affected by heat-accumulating wall

Covering ways of pipes

Based on the above research, the effect of covering ways was also verified by experiments. The black and white plastic film were, respectively, covered on the pipes, and the distance between the pipes and the heat-accumulating wall is 100 mm, and then the heights of pipes and the ground are changed at different days, which are -35 mm, -15 mm, 0 mm, 20 mm, 40 mm, and 65 mm. In this experiment, when the distance between the outer wall

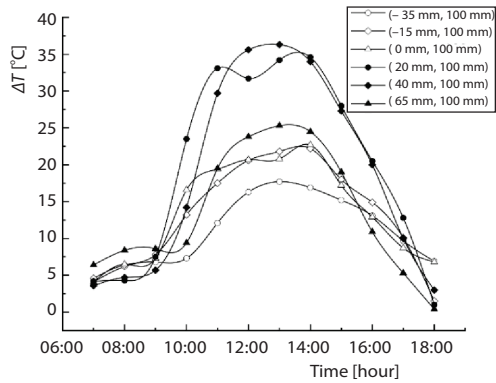


Figure 9. Curves of the difference between water temperature in pipes and air temperature at different distances from pipe bottom to ground and heat-accumulating wall

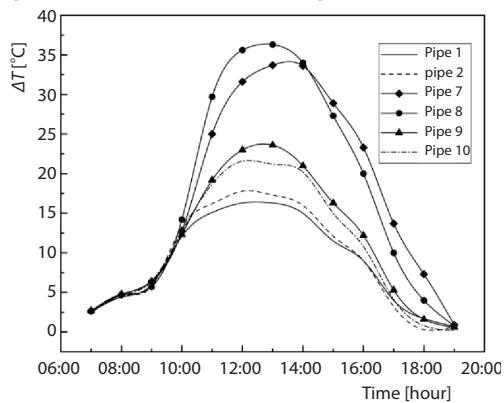


Figure 10. Curves of the difference between water temperature in pipes and air temperature on September 22

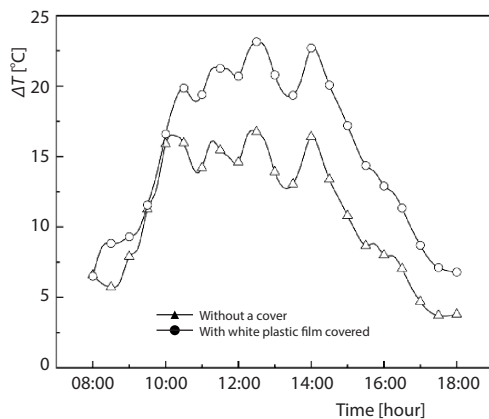


Figure 11. Comparison of the effect of coverage and no cover on water temperature on September 17

of the black PE pipe covered with white plastic film and the heat-accumulating wall and the ground is 100 mm and 40 mm, respectively, the water in the pipe obtains the highest heat in this experiment, and the difference between the water temperature in the pipe and the air temperature reaches 36.3 °C. When the distance between the outer wall of the black PE pipe covered with white plastic film and the heat gathering wall and the ground is 100 mm and 20 mm, respectively, the sub-high heat of the test was obtained from the water in the pipe, and the difference between the water temperature in the pipe and the air temperature reached 34.8 °C. Figure 9 shows the difference between water temperature (Pipe 8) and ambient air temperature at different heights from the bottom of the pipe to the sand floor. It can be seen that the solar radiation has the greatest impact on the heat collection of pipes, and the white plastic film has a greater impact on the heat collection of pipes. The optimum distance between overhead pipe-lines and the ground is 0.90~1.25 times of the outer diameter of pipes.

Figure 10 is the test curve of September 22. Pipe 1 and Pipe 2 are bare on sand, and the overhead heights of Pipe 7, Pipe 8, Pipe 9, and Pipe 10 are 40 mm under the same weather conditions. In fig. 10, the order of water temperature in each pipe is: $T_{\text{Pipe 8}} > T_{\text{Pipe 7}} > T_{\text{Pipe 9}} > T_{\text{Pipe 10}} > T_{\text{Pipe 2}} > T_{\text{Pipe 1}}$. It can be seen that the heat gain of pipe covered with white plastic film is greater than that covered with black plastic film. This is because the white plastic film has good transparency and can obtain more heat, and the closed region formed with the ground reduces the heat disperse of air convection, improving the ground temperature, which plays a good role in thermal insulation.

In order to further verify the effect of coverage, this paper compares and analyzes the difference between measured water temperature and atmospheric temperature in Pipe 8 and Pipe 2, which are placed on the surface under the same weather conditions. It can be seen from fig. 11 that under the same weather conditions, the trend of water temperature in the two tubes

are consistent. After 10:00 o'clock, Pipe 8 increased the temperature significantly more than Pipe 2, and the temperature difference between the two reached 7.0 °C, with an average temperature difference of 4.4 °C. It can be seen that under the action of covering, the warming amplitude of water temperature is obvious, which reduces the heat loss caused by natural-convection between the air and the outer wall of the pipe, thus improving the water temperature.

The effect of weather condition

In order to investigate the influence of weather conditions on the experimental results, this paper compares the measured water temperatures under sunny and cloudy weather, when the Pipe 5 mm is 65 mm from the wall and the ground. The data in fig. 12 is obtained by measuring the difference between the measured water temperature and the real-time atmospheric temperature of the day, which can be seen that the water temperature under sunny conditions is significantly higher than that under cloudy weather conditions. After 10:00 o'clock, with the increase of the solar altitude angle, the solar radiation gradually increases, and the difference between the water temperature under sunny days and cloudy days increases, with the maximum temperature difference between the two reaching 12 °C and the average temperature difference of 6.5 °C. It also can be seen that cloudy weather weakens the solar radiation intensity, reducing the heat gain of the pipe, which is not conducive to the increase of water temperature in the pipe.

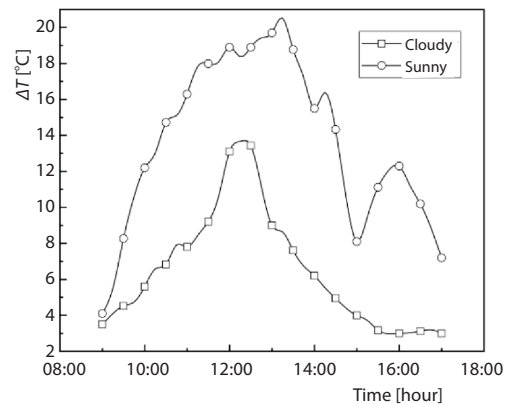


Figure 12. Water temperature under different weather conditions

After 10:00 o'clock, with the increase of the solar altitude angle, the solar radiation gradually increases, and the difference between the water temperature under sunny days and cloudy days increases, with the maximum temperature difference between the two reaching 12 °C and the average temperature difference of 6.5 °C. It also can be seen that cloudy weather weakens the solar radiation intensity, reducing the heat gain of the pipe, which is not conducive to the increase of water temperature in the pipe.

Numerical simulating analysis

Introduction ANSYS FLUENT 16.0

The FLUENT is a computer program for simulating the fluid-flow and heat conduction of complex shapes, which is one of the CFD software with comprehensive functions, strong applicability and extensive use in China. Flexible unstructured grids and mature physical models make FLUENT software widely used in laminar flow, turbulence, heat transfer, phase transition, multi-phase flow, *etc.* The FLUENT software is composed of two core parts: pre-processing software such as (ICEM CFD, Gambit, FLUENT Meshing, and Turbo Grid) and post-processing solver. In GAMBIT, the steps of establishing geometric model and generating grid are carried out, while FLUENT completes the process of setting object boundary conditions, initializing and solving. In this study, besides the convective heat transfer between the pipe wall and the water, the effects of solar radiation and radiative heat transfer between the surfaces are also considered.

Numerical simulation

Physical model

In order to further verify the effects of the pipe material, the spatial position of pipes, covering ways of pipe and heat accumulating wall in the field test, a 3-D model was established to simulate the variation and characteristics of water temperature in each pipe under certain environmental space.

The material and size specifications of the pipes' model are consistent with the test, see tab. 1. The external air-flow area is 10 m long, 8 m wide, and 8 m high, with the east-west direction in the length direction and the north-south direction in the width direction; The velocity inlet is east and the pressure outlet is west, see fig. 13. The size of the heat-collecting wall model is 4 m long, 0.3 m wide, and 0.55 m high. The pipe and the heat-collecting wall model are located at the center of the air basin, and the x-axis is positive to the East. For the sake of simplicity of calculation, following assumptions were taken out:

- The flow is incompressible.
- Fluid thermal properties are considered constant throughout the flow.
- The thickness of the plastic film wrapped around the outer wall of the pipe is negligible.

The physical properties of the materials are shown in tab. 2.

Table 2. List of thermo physical properties

Physical parameters	Air	Water	Galvanized steel	PE plastic pipes	Sand
Density [kgm^{-3}]	1.23	998.20	8030	950	1925
Specific heat capacity [$\text{Jkg}^{-1}\text{K}^{-1}$]	1006.40	4182	502.48	2301	900
Thermal conductivity [$\text{Wm}^{-1}\text{K}^{-1}$]	0.02	0.60	54	0.48	2.30

Mathematical model

Governing equations

In this study, the natural-convection and heat transfer occur between the outer wall of the pipe and the air in the outer large space area, while there is no relative flow between the inner wall of the pipe and the water, and heat transfer is mainly carried out by means of heat conduction. Therefore, the fluid-flow and heat transfer in the computational domain need to satisfy the following basic governing equations [23, 24].

Mass conservation equation:

$$\frac{\partial u_x}{\partial x} + \frac{\partial u_y}{\partial y} + \frac{\partial u_z}{\partial z} = 0 \quad (3)$$

Momentum conservation equation:

- X-direction momentum conservation

$$\frac{\partial \rho u_x}{\partial t} + \nabla(\rho u_x \bar{u}) = -\frac{\partial p}{\partial x} + \frac{\partial \tau_{xx}}{\partial x} + \frac{\partial \tau_{yx}}{\partial y} + \frac{\partial \tau_{zx}}{\partial z} + F_x \quad (4)$$

- Y-direction momentum conservation

$$\frac{\partial \rho u_y}{\partial t} + \nabla(\rho u_y \bar{u}) = -\frac{\partial p}{\partial y} + \frac{\partial \tau_{xy}}{\partial x} + \frac{\partial \tau_{yy}}{\partial y} + \frac{\partial \tau_{zy}}{\partial z} + F_y \quad (5)$$

- Z-direction momentum conservation

$$\frac{\partial \rho u_z}{\partial t} + \nabla(\rho u_z \bar{u}) = -\frac{\partial p}{\partial z} + \frac{\partial \tau_{xz}}{\partial x} + \frac{\partial \tau_{yz}}{\partial y} + \frac{\partial \tau_{zz}}{\partial z} + F_z \quad (6)$$

where p [Pa] is the pressure, ρ [kgm^{-3}] – the fluid density, τ_{xx} , τ_{xy} , τ_{xz} , τ_{yx} , τ_{yy} , τ_{yz} , τ_{zx} , τ_{zy} , τ_{zz} are all components of stress tensors, F_x , F_y , and F_z – the physical forces on the micro-element. If the physical force is only gravity, and the z-axis is vertical, $F_x = 0$, $F_y = 0$, $F_z = -\rho g$.

Energy conservation equation:

$$\frac{\partial(\rho E)}{\partial t} + \nabla[\bar{u}(\rho E + p)] = \nabla\left[\lambda_{\text{eff}}\Delta T - \sum_j h_j J_j + (\tau_{\text{eff}}\bar{u})\right] + S_h \quad (7)$$

where ρ [kgm^{-3}] is the fluid density, E [Jkg^{-1}] – the total energy of the fluid micelle, which is the sum of internal energy, kinetic energy, and potential energy, p [Pa] – the pressure, λ_{eff} [$\text{Wm}^{-1}\text{K}^{-1}$] – the effective thermal conductivity, T [K] – the temperature, h [Jkg^{-1}] – the enthalpy, h_j [Jkg^{-1}] – the enthalpy of component j , J_j [Jkg^{-1}] – the diffusive flux of component j , τ_{eff} – coefficient of the effective viscosity, \bar{u} – the fluid velocity, and S_h [Wm^{-3}] – the source term of volumetric heat.

Turbulent model

For the flow in the air zone, a standard k - ε turbulent model is set and the inlet velocity is the average wind speed during the experimental period on August 25, which is 2.0 m/s, being based on the real-time observed data from the China Meteorological Administration.

The turbulent energy, k , and the dissipative rate, ε , equation of the standard model are:

$$\rho \frac{Dk}{Dt} = \frac{\partial}{\partial x} \left[\left(\mu + \frac{\mu_t}{\sigma_k} \right) \frac{\partial k}{\partial x} \right] + G_k + G_b - \rho\varepsilon \quad (8)$$

$$\rho \frac{D\varepsilon}{Dt} = \frac{\partial}{\partial x} \left[\left(\mu + \frac{\mu_t}{\sigma_k} \right) \frac{\partial \varepsilon}{\partial x} \right] + C_{1\varepsilon} \frac{\varepsilon}{k} (G_k + C_{3\varepsilon} G_b) - C_{2\varepsilon} \rho \frac{\varepsilon^2}{k} \quad (9)$$

The coefficient of turbulent viscosity:

$$\mu_t = \rho C_\mu \frac{k^2}{\varepsilon} \quad (10)$$

where k [J] is the turbulent energy, ε – the dissipative rate, μ [$\text{Pa}\cdot\text{s}$] – the viscosity, μ_t – the coefficient of turbulent viscosity, G_k [J] – the turbulent energy generated by the mean velocity gradient, G_b [J] – the turbulent energy generated by buoyancy, ρ [kgm^{-3}] – the fluid density, σ_k – the Prandtl number of turbulence, whose value is equal to 1.0. The model constants used in the simulation are $C_{1\varepsilon} = 1.44$, $C_{2\varepsilon} = 1.92$, $C_{3\varepsilon} = 1.0$, $C_\mu = 0.09$.

Radiant model

The ray tracing algorithm using the solar loading model and the P1 radiant model simulate the effects of solar radiation and the radiative heat transfer between the surfaces. Because of the large optical thickness of the atmospheric boundary-layer in this study, it is also necessary to consider the scattered radiation and the time-consuming factors of calculation. Therefore, the P1 model is used for calculation, which of the general radiative energy equation can be approximated as the diffusion flux equation, allowing for a simpler calculation and demanding less computational power from the CPU [25].

Radiant heat flow, q :

$$q = -\frac{1}{3(\alpha + \sigma_s) - B\sigma_s} \nabla I_i \quad (11)$$

where α is the absorption coefficient σ_s – the scattering coefficient, I_i [Wm^{-2}] – the incident radiation, and B – coefficient of phase function with linear anisotropy.

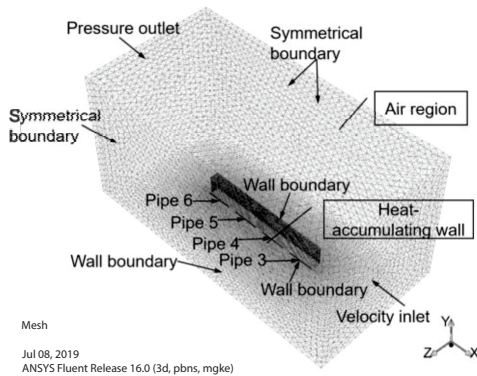


Figure 13. Geometric model and boundary conditions

Heat-accumulating wall

Based on the relative position between the wall and the pipe in the test, the model of the heat-accumulating wall is set as the wall boundary to consider the effect of radiative heat transfer between the wall and the pipe on the water temperature inside the tube.

Pipes' model

According to the spatial position of pipes in the experiment, the bottom surface of the pipe model is 40 mm away from the ground and the heat-accumulating wall in the numerical model. Wall boundary is adopted on all surfaces of the pipe, and water is used as the working medium inside. The mesh generation is denser than the external large space, so as to obtain a more accurate distribution of pipes' superficial temperature and the temperature of the water in the pipe.

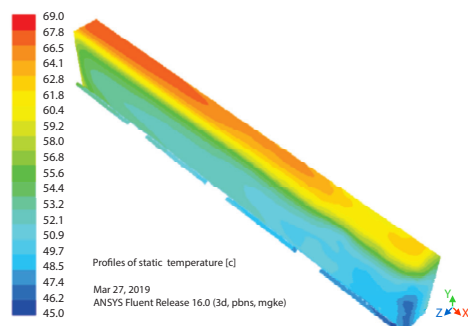


Figure 14. The simulation of temperature field at 02:00 p. m. (for color image see journal web site)

is basically consistent with the temperature distribution of heat-accumulating wall, indicating that heat-accumulating wall has a significant effect on the change of water temperature inside the pipes. Comparing the measured values with the simulated values, it can be observed that the results are basically consistent, and the accuracy of the simulated results is also reflected to some extent.

Boundary conditions

In GAMBIT, the models of pipes, heat-accumulating wall and air region are established to simulate the effects of air-flow and solar radiation in the atmospheric boundary-layer on the temperature field of water in pipe. The Geometric model and boundary conditions are shown in fig. 13.

Air region

External large space is an air basin with velocity inlet and pressure outlet to simulate air-flow and symmetrical boundary around the basin. The bottom of the large space is the ground, which is set to the wall boundary [26], considering the effect of radiative heat transfer on the temperature of pipes.

The FLUENT solution and analysis

The output mesh is imported into the 3-D solver of FLUENT for solution calculation. In the solar calculator, the simulated time is set to 02:00 p. m. on August 25. Simple algorithm is used to solve the pressure-velocity coupling equation, the second-order upwind scheme is chosen for time and energy, the first-order upwind scheme for turbulent and radiant equation, and the appropriate sub-relaxation factor is selected. The results of the numerical model are shown in fig. 14.

It can be observed from fig. 14 that the temperature distribution of the water in the pipes

The model of temperature prediction

Multivariate linear regressive model

On the basis of the heat transfer test, the test method and measured data of the black PE pipe covered by the white plastic film at a distance of 100 mm from the heat-accumulating wall and 40 mm above the ground were selected to establish a multivariate linear regressive model, and then to realize the prediction of water temperature.

According to the principle of multivariate regressive analysis, the mathematical model of dependent variable and independent variable are established eq. (12):

$$y = a_0 + a_1x_1 + a_2x_2 + a_3x_3 + \dots + a_mx_m \quad (12)$$

where y is the dependent variable, x – the independent variable, a_0 – the constant, a_m – the regressive coefficient, and m – the represents number of independent variables, $m = 1, 2, 3, 4, \dots$

There are many factors affecting the change of water temperature in the pipes, such as weather conditions, atmospheric temperature, air humidity, solar radiant intensity and so on. Through the correlative analysis of the measured data and the observation data, two significant environmental factors, atmospheric temperature and solar radiant intensity, are selected as the correlative factors.

According to the regressive analysis, T_p represents the predicted water temperature inside the tube. The SPSS software was used to analyze and obtain $a_0 = 5.22$, $a_1 = 0.315$, and $a_2 = 0.09$, eventually obtaining the predictive regressive model of water temperature in the pipe eq. (13):

$$T_p = 0.315T_a + 0.09I_r + 5.22 \quad (13)$$

where T_p [°C] is the predicted water temperature inside the pipe, T_a [°C] – the measured atmospheric temperature at a certain moment, I_r [Wm^{-2}] – the intensity of solar radiation at a certain moment, a_0 – the constant related to the regressive equation, a_1 – the regressive coefficient relating to atmospheric temperature, and a_2 – the regressive coefficient relating to solar radiation intensity.

Table 3 shows the results of significance test of the regressive equation by ANOVA [27]. It can be observed that the mean square of the regressive equation is 3790.50, and the mean square of the residual is 1.466. The F of the F test is $F = 2585.5 > F_{0.05}(2, 41) = 3.226$, and $Sig = 0.000 < 0.01$, indicating that the regressive equation is significant.

Table 3. Variance analysis

Model	Sum of squares	Degrees of freedom	Mean square	F
Regression	7581.00	2	3790.50	2585.5
Residual	57.18	39	1.466	
Total	7638.18	41		

Verification and analysis of predictive model

The predictive values were calculated by substituting the measured atmospheric temperature and the data of solar radiant intensity on September 22 into the multivariate regressive model, compared with the water temperature in the measured pipe. It can be observed from fig. 15 that the predicted value of the multivariate linear regressive model is in good agreement with the water temperature in the measured pipe, and the trend of the curve is consistent.

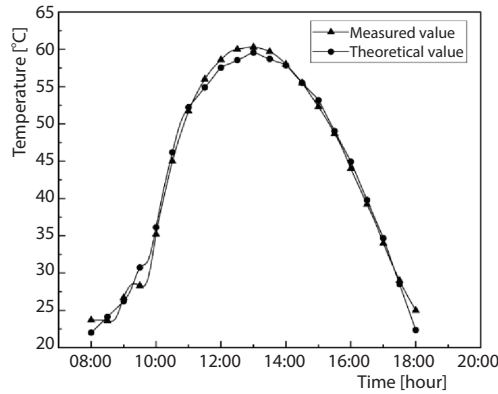


Figure 15. Comparison of predicted and measured water temperature in pipe

In order to further verify the accuracy of the regressive model, this paper utilizes the mean error, the mean absolute error, the mean relative error and other indicators as a measure of predictive accuracy:

– mean error (ME):

$$ME = \frac{\sum_{i=1}^n T_{pi} - \hat{T}_{pi}}{n} \quad (14)$$

– mean absolute error (MAE):

$$MAE = \frac{\sum_{i=1}^n |T_{pi} - \hat{T}_{pi}|}{n} \quad (15)$$

– mean relative error (MRE):

$$MRE = \frac{1}{n} \sum_{i=1}^n \frac{T_{pi} - \hat{T}_{pi}}{T_{pi}} \quad (16)$$

– mean absolute percentage error (MAPE):

$$MAPE = \frac{1}{n} \sum_{i=1}^n \left| \frac{T_{pi} - \hat{T}_{pi}}{T_{pi}} \right| \quad (17)$$

where T_{pi} [°C] is the predictive water temperature, \hat{T}_{pi} [°C]– the measured water temperature, i is the ordinal number of value.

According to the water temperature predicted by the binary linear regressive predictive model and measured values, the $ME = 0.033$, the $MAE = 0.92$, the $MRE = 0.065$, the $MAPE = 0.023 = 2.3\%$. It can be seen that the accuracy of the predictive model is high.

Conclusions

Through practical experiment and numerical analysis, this paper discusses the variation of shallow geo-temperature and the heat transfer characteristics of aboveground pipes under the solar radiation. The results of numerical simulation agree generally well with experimental data. Thereby, the predicting model of water temperature is established, and the following conclusions are obtained.

- The heat gain of the water in the pipe is most significantly affected by the intensity of solar radiation, and is also related to the color of the pipe and its spatial location. When the galvanized steel pipe wrapped with black plastic film has an overhead height of 40 mm, the difference between the water temperature in the pipe and the atmospheric temperature reaches a maximum value of 20.9 °C.
- The heat-accumulating wall can effectively raise the water temperature inside the pipe. Under the action of solar radiation, when the galvanized steel pipe wrapped with black plastic film is 40 mm away from the heat-accumulating wall and the sand floor, its water temperature is higher than that of pipe without heat-accumulating wall at 5-10 °C.
- The way the pipe is covered has a great influence on the water temperature inside the pipe. When the black PE pipe covered with the white plastic film is in the best space position, the highest heat of the three series of tests is obtained, and the difference between the water temperature inside the pipe and the atmospheric temperature reaches 36.3 °C.

- The numerical model of heat transfer established by ANSYS FLUENT software can better reflect the actual situation of temperature field.
- This research synthetically utilizes solar radiant heat, reflective heat of structure, heat flow and covering thermal insulation, providing a new way for efficient utilization of solar energy to produce large quantities of hot water.

Acknowledgment

This work was supported by the Key R and D Projects (the High and New Domain) of Shanxi Province in 2018 under Grant (No. 201803D121112). This support is gratefully acknowledged.

Nomenclature

a_0 – constant used in eq. (13), [–]
 a_1, a_2 – regressive coefficient, [–]
 B – coefficient of phase function, [–]
 C_{1e}, C_{2e} – empirical constant, [–]
 C_{3e}, C_{μ} – empirical constant, [–]
 C_u – coefficient uniformity, [–]
 C_c – coefficient of curvature, [–]
 DN – inner diameter, [m]
 D – outer diameter, [m]
 E – total energy, [J]
 F – physical forces, [$\text{kgm}^{-1}\text{s}^{-2}$]
 G_k – turbulent energy generated by the mean velocity gradient, [J]
 G_b – turbulent energy generated by buoyancy, [J]
 H – heat transfer coefficient, [$\text{Wm}^{-2}\text{C}^{-1}$]
 h – enthalpy, [Jkg^{-1}]
 h_j – enthalpy of component j , [Jkg^{-1}]
 I_a – solar radiant intensity absorbed by the pipe, [Wm^{-2}]
 I_i – incident radiation, [Wm^{-2}]
 I_r – intensity of solar radiation, [Wm^{-2}]
 i – ordinal number of value, [–]
 J_j – diffusive flux of component j , [Jkg^{-1}]
 k – turbulent energy, [J]
 L – length of pipe, [m]
 m – number of independent variables, [–]
 n – normal direction of the pipe's surface, [–]
 p – pressure, [kPa]
 q_f – heat flux density, [Wm^{-2}]
 S_h – source term of volumetric heat, [Wm^{-3}]
 T_w – wall temperature of the pipe, [$^{\circ}\text{C}$]
 T_f – fluid temperature, [$^{\circ}\text{C}$]
 T_s – effective temperature of the sky, [K]

T_g – ground temperature, [K]
 T_h – temperature of heat-accumulating wall, [K]
 T_p – predicted water temperature inside the pipe, [$^{\circ}\text{C}$]
 T_a – measured atmospheric temperature at a certain moment, [$^{\circ}\text{C}$]
 \hat{T}_{pi} – measured water temperature inside the pipe at a certain moment, [$^{\circ}\text{C}$]
 \vec{u} – velocity vector, [–]
 u_x, u_y, u_z – velocity of y -direction, [ms^{-1}]

Greek letters

α – absorption coefficient, [–]
 δ – wall thickness, [m]
 ε – dissipative rate, [–]
 ε_f – emissivity, [–]
 λ – thermal conductivity, [$\text{Wm}^{-1}\text{K}^{-1}$]
 λ_{eff} – effective thermal conductivity, [$\text{Wm}^{-1}\text{K}^{-1}$]
 μ – viscosity, [$\text{kgm}^{-1}\text{s}^{-1}$]
 μ_t – coefficient of turbulent viscosity, [$\text{Pa}\cdot\text{s}$]
 ρ – fluid density, [kgm^{-3}]
 σ – Stefan-Boltzmann constant, [$\text{kgs}^{-3}\text{K}^{-4}$]
 σ_k – Prandtl number of turbulence, [–]
 σ_s – scattering coefficient, [–]
 τ_{eff} – coefficient of the effective viscosity, [–]
 $\tau_{xx}, \tau_{xy}, \tau_{xz}$ – components of stress tensors, [–]
 $\tau_{yx}, \tau_{yy}, \tau_{yz}$ – components of stress tensors, [–]
 $\tau_{zx}, \tau_{zy}, \tau_{zz}$ – components of stress tensors, [–]
 ϕ_{wg} – angular coefficient between the pipe's surface and the ground, [–]
 ϕ_{wh} – angular coefficient between the surface and heat-accumulating wall, [–]
 ϕ_{ws} – angular coefficient between the pipe's surface and the sky, [–]

References

- [1] Kumar, A., *et al.*, Experimental Investigation of an Air Heating System Using Different Types of Heat Exchangers Incorporated with an Evacuated Tube Solar Collector, *Environmental Progress and Sustainable Energy*, 36 (2017), 1, pp. 232-247
- [2] Huo, Z., *et al.*, Research Report on Development of China Solar Thermal Industry (in Chinese), *Proceedings, Annual Conference and Summit Forum of China Solar Energy Thermal Utilization Industry in 2011*, China Solar Thermal Industry Federation, Xi'an, China, 2011
- [3] Liu, G., *et al.*, Effect of Different Installation Tilt Angles on Electricity Yield in PV Power Station (in Chinese), *Acta Energetica Solaris Sinica*, 36 (2016), 12, pp. 2973-2978

- [4] Recalde, C., et al., Effect of Tilt Angle of Evacuated Tubes on the Temperature of the Water, *Informacion Tecnologica*, 26 (2015), 4, pp. 89-96
- [5] Tang, R., et al., Optimal Tilt-Angles of All-Glass Evacuated Tube Solar Collectors, *Energy*, 34 (2009), 9, pp. 1387-1395
- [6] Vall, S., et al., Energy Savings Potential of a Novel Radiative Cooling and Solar Thermal Collection Concept in Buildings for Various World Climates, *Energy Technology*, 6 (2018), 11, pp. 2200-2209
- [7] Bracamonte, J., et al., Effect of The Collector Tilt Angle on Thermal Efficiency and Stratification of Passive Water in Glass Evacuated Tube Solar Water Heater, *Applied Energy*, 155 (2015), Oct., pp. 648-659.
- [8] Huang, J. B., et al., Experimental Investigation on Thermal Performance of Thermosyphon Flat-Plate Solar Water Heater with a Mantle Heat Exchanger, *Energy*, 35 (2010), 9, pp. 3563-3568
- [9] Yakup, M. A. B. H. M., Malik, A. Q., Optimal Tilt-Angle and Orientation for Solar Collectors in Brunei, Darussalam, *Renewable Energy*, 24 (2001), 2, pp. 223-234.
- [10] Zhao, J., et al., Calculation and Analysis of the Optimum Angle of Solar Collectors in Lanzhou (in Chinese), *Building Energy Efficiency*, 47 (2019), 1, pp. 28-31
- [11] Despotovic, M., Nedic, V., Comparison of Optimum Tilt Angles of Solar Collectors Determined at Yearly, Seasonal and Monthly Levels, *Energy Conversion and Management*, 97 (2015), June, pp. 121-131
- [12] Khan, M. M. A., et al., Evaluation of Solar Collector Designs with Integrated Latent Heat Thermal Energy Storage: A Review, *Solar Energy*, 166 (2018), May, pp. 334-350
- [13] Lin, S. C., et al., Experiment Investigation on the Performance Enhancement of Integrated PCM-Flat Plate Solar Collector, *Journal of Applied Sciences*, 23 (2012), 12, pp. 2390-2396
- [14] Abuska, M., et al., Experimental Analysis of Solar Air Collector with PCM-Honeycomb Combination Under the Natural Convection, *Solar Energy Materials and Solar Cells*, 195 (2019), June, pp. 299-308
- [15] Romnn-Roldan, N. I., et al., Computational Fluid Dynamics Analysis of Heat Transfer in a Greenhouse Solar Dryer Chapel-Type Coupled to an Air Solar Heating System, *Energy Science and Engineering*, 7 (2019), 4, pp. 1123-1139
- [16] Tanha, K., et al., Simulation and Experimental Investigation of Two Hybrid Solar Domestic Water Heaters with Drain Water Heat Recovery, *Int. J. Energy Res.*, 39 (2015), 14, pp. 1879-1889
- [17] Benoit, H., et al., Three-Dimensional Numerical Simulation of up-Flow Bubbling Fluidized Bed in Opaque Tube uner High Flux Solar Heating, *American Institute of Chemical Engineers*, 64 (2018), 11, 3857-3867
- [18] Alfaro-Ayala, J. A., et al., Numerical Study of a Low Temperature Water-in-Glass Evacuated Tube Solar Collector, *Energy Conversion and Management*, 94 (2015), Apr., pp. 472-481
- [19] Morrison, G. L., et al., Water-in-Glass Evacuated Tube Solar Water Heaters, *Solar Energy*, 76 (2004), 1-3, pp. 135-140
- [20] Selmi, M., et al., Validation of CFD Simulation for Flat Plate Solar Energy Collector, *Renewable Energy*, 33 (2008), 3, pp. 383-387
- [21] Charvat, P., et al., Solar Air Collector with the Solar Absorber Plate Containing a PCM Environmental Chamber Experiments and Computer Simulations, *Renewable Energy*, 143 (2019), Dec., pp. 731-740
- [22] Ayompe, L. M., et al., Comparative Field Performance Study of Flat Plate and Heat Pipe Evacuated Tube Collectors (Etc) for Domestic Water Heating Systems in a Temperate Climate, *Energy*, 36 (2011), 5, pp. 3370-3378
- [23] Tao, W., et al., *Heat Transfer* (in Chinese), 4th ed., Higher Education Press, Beijing, China, 2006
- [24] Han, Z. Z., et al., *The FLUENT Fluid Engineering Emulator Calculation Example and Application* (in Chinese), Beijing Institute of Technology Press, Beijing, China, 2004
- [25] Kuharat, S., et al., Computational Study of Heat Transfer in Solar Collectors with Different Radiative Flux Models, *Energy Technology*, 48 (2019), 3, pp. 1002-1031
- [26] Xiao, X., Experimental and Numerical Study on Temperature of Steel Members and Single-Layer Lattice Shell Considering Coupling of Radiation, Thermal and Fluid (in Chinese), M. Sc. thesis, Tianjin University, China, 2014
- [27] Duan, X. S., et al., Multiple Linear Regression Analysis Method for in-Situ Thermal Conductivities of Rock and Soil Layer (in Chinese), *Acta Energiæ Solaris Sinica*, 39 (2018), 2, pp. 385-389